Department of Physics and Astronomy
University of Heidelberg

Bachelor Thesis in Physics
submitted by

David Fischer

born in Heidelberg (Germany)

2015

Analysis of a 2-D-Bose-Hubbard Model

This Bachelor Thesis has been carried out by David Fischer at the
Institute of Theoretical Physics in Heidelberg
under the supervision of
PD Dr. Sandro Wimberger

Abstract

The Bose-Hubbard model offers both theoretically and experimentally a great access to studies of bosonic many-body-systems in periodic potentials. In this thesis we will apply it to a two-dimensional lattice consisting of 2×2 potential pots. The first part of our studies will concern the spectral characteristics of different 2×2 systems and particularly the influence of their geometry. Motivated by current experimental observations of the refilling process in a Bose-Hubbard chain after one lattice site is emptied, we will then proceed by opening the system in the second part. By use of a master equation approach, we investigate the impact of different kinds of interactions with the environment on the dynamics of the system.

Zusammenfassung

Das Bose-Hubbard-Modell stellt sowohl theoretisch als auch experimentell einen guten Zugang zur Beschreibung bosonischer Viel-Teilchen-Systeme in periodischen Potentialen dar. In dieser Arbeit werden wir es auf ein zweidimensionales Gitter, bestehend aus 2×2 Potentialtöpfen, anwenden. Der erste Teil unser Untersuchungen betrifft die spektralen Eigenschaften verschiedener 2×2-Systeme und den Einfluss, den deren Geometrie dabei spielt. Motiviert durch aktuelle experimentelle Beobachtungen von Auffüll-Prozessen in einer eindimensionalen Bose-Hubbard-Kette, nachdem ein Gitterplatz geleert wurde, werden wir im zweiten Teil dazu übergehen, das System zu öffnen und die Auswirkung verschiedener Arten von Wechselwirkungen mit der Umgebung auf die Dynamik des Systems betrachten.

Contents

Chapter 1

Introduction and Motivation

While the Bose-Hubbard model for bosonic many body systems in periodic, one-dimensional lattices already has undergone extensive analysis [1, 2, 3], recently these examinations have been extended to higher-dimensional setups as well [4, 5]. The model-systems we will consider throughout this thesis will be two-dimensional lattices consisting of 2×2 sites.

After the introduction of the theoretical framework necessary for our examinations (chapter 2), in section 3.1, we will construct a model in order to simulate a refilling process, observed in a one-dimensional Bose-Hubbard chain in recently performed experiments [6]. Here the spacial extend of the lattice sites complicates the situation such that the refilling dynamics can not easily be described by the one-dimensional model. We will try to solve this problem by implementing a virtual pot corresponding to a higher excited state. Section 3.2 is dedicated to a general analysis of the spectral properties of 2×2- Bose-Hubbard Hamiltonians dependent on the structure of the couplings between the sites. We will then proceed by opening our model system and numerically simulate the dynamics under different forms of interactions with the environment governed by a master equation approach.
Due to efficiency reasons we will rely on the quantum jump method for all calculations in those simulations.

Chapter 2

Theoretical Foundation

2.1 Master Equation Formalism

The description of a quantum system as a state-vector evolving in time is in fact an approximation, where we assume the system to be closed from its environment. In reality this is never possible to be achieved and while in certain cases the effects that arise from couplings to the environment can be neglected, we want to focus on systems where they have a great influence on the behavior and therefore require a density matrix approach.

Although the dynamics of such a system cannot be written in terms of a unitary time evolution given by the Hamilton operator H, it is still possible to formulate the Master Equation in Lindblad form for the density matrix ϱ preserving trace and positivity of ϱ [7].

$$\dot{\varrho} = -\frac{i}{\hbar}[H, \varrho] + \mathcal{L}[\varrho] \tag{2.1}$$

Here the Born-Markov approximation is used that requires the environment to have "a weak memory", meaning that correlations in the reservoir decay much faster than the typical timescale of our system [7].
$\mathcal{L}[\varrho]$ - the Liouvillian - is taking into account that our system is open and can be written in the form:

$$\mathcal{L}[\varrho] = \sum_i \gamma_i (A_i \varrho A_i^\dagger - \frac{1}{2} A_i^\dagger A_i \varrho - \frac{1}{2} \varrho A_i^\dagger A_i) \tag{2.2}$$

The A_i are the Lindblad operators and represent dissipation processes, while the γ_i give the rates, at which those occur.
As one would expect, by setting $\mathcal{L}[\varrho] = 0$, one obtains the von Neumann equation valid for a closed system.

Our first goal will therefore be to find a suitable model for H, to simplify the problem as far as possible and to understand the unitary dynamics. Then we will proceed by investigating the effects of added dissipative processes.

2.2 The Bose-Hubbard Model

The quantum system we consider throughout this thesis will be a bosonic many-body-system in a periodic, sufficiently deep potential, so that a tight binding approximation can be applied and only the lowest Bloch band is occupied [8]. Experimentally this can be realized with ultra-cold atoms in an optical lattice.
In such a case accurate predictions of the dynamics can be made by use of the Bose-Hubbard model, claiming H to be of the following form in second quantization formalism [8]:

$$H = \sum_{n=1}^{L} \epsilon_i n_i + \frac{U}{2} \sum_{i=1}^{L} n_i(n_i - 1) - \sum_{i=1}^{L} \sum_{j=1}^{i} J_{ij}(a_i^\dagger a_j + a_j^\dagger a_i) \tag{2.3}$$

where $n_i = a_i^\dagger a_i$ and $a_i^\dagger, a_i$ are the creation and annihilation operator for the i-th site of the periodic lattice, obeying the bosonic commutation relation $[a_j, a_i^\dagger] = \delta_{ij}$.

Each term in this sum has an intuitively accessible meaning: The ϵ_i correspond to an on-site potential, U is the interaction strength between particles in the same well and $J_{ij} = J_{ji}$ is the tunneling-coefficient between the i-th and j-th site.
While in the standard 1-D-Bose-Hubbard model ($J_{ij} = \delta_{1,|j-i|}$) the sites are ordered along a chain, we consider a more general form, keeping it open which sites to couple.

In the latter we will always refer to the number of sites as L and consider states with the total particle number $N = \sum_{n=1}^{L} n_i$, which is conserved by the Hamiltonian time evolution because $[H, N] = 0$.
This allows us to perform all calculations in the finite dimensional subspace of the Fock space spanned by states of the form[1]:

$$\begin{gathered} |0, 0, ..., 0, N\rangle \\ |0, 0, ..., 1, N-1\rangle \\ |0, 0, ..., 2, N-2\rangle \\ \vdots \\ |N, 0, ..., 0\rangle \end{gathered}$$

The dimension D of this subspace is the number of possibilities to distribute N particles to L sets:

$$D = \binom{N + L - 1}{N} = \frac{(N + L - 1)!}{N!(L - 1)!} \tag{2.4}$$

In that way the Schrödinger equation and the von Neumann equation become systems of D or D^2 ordinary differential equations (ODEs), respectively.

[1] At this point the recursive structure of the basis should be noted:
$basis(N, L) = \{\{(i)\} \otimes basis(N - i, L - 1) \ for \ i \leq N\}$

2.3 Symmetries and Spectral Statistics

Symmetries can be used to cancel out redundancies in the description of a system. In our case we will find symmetry operators S, which commute with the Hamiltonian of the system: $[H, S] = 0$
As the spectral theorem states, we then can find an orthonormal basis $\mathcal{B}$ of the Hilbert space, built from eigenvectors of both H and S. By ordering the basis with respect to the eigenvalues of S and applying a basis transformation to this reordered basis $U_{\mathcal{B}'}$, it can be achieved that the Hamilton operator has block form, each block H_i related to an eigenvalue of the symmetry.

$$U_{\mathcal{B}'} H U_{\mathcal{B}'}^{-1} = \begin{pmatrix} H_1 & & \cdots & 0 \\ & H_2 & & \vdots \\ \vdots & & \ddots & \\ 0 & & \cdots & H_k \end{pmatrix} \tag{2.5}$$

There are two reasons for doing this: First, when we choose our starting state to obey the same symmetry, it is sufficient to consider only one block for the time evolution of this state and therefore we can reduce the numerical effort of the integration.
The second reason is that we want to analyze the behaviour of the system concerning chaos or regularity. Our methods of choice use results from Random Matrix Theory (RMT) [9] to compare the following three quantities of the spectrum with predicted statistics.
As a first indicator we will observe the nearest neighbour spacings in the spectrum. For reasons of comparability to the RMT predictions we have to separate this local property from global trends in the spectrum. This has to be done through a suitable rescaling, normalizing the average spectral density $\bar{\rho} = 1$ and therefore dismissing the global trend without loosing the information about local fluctuations. This technique is called the unfolding [10] of the spectrum.
It can be shown that in an integrable system, the energy levels are distributed independently. This results in Poisson-distributed spacings s [11]:

$$P_{\text{Pois}}(s) = e^{-s} \tag{2.6}$$

The chaotic case can be described by an ensemble of random matrices $\{H_R\}$, obeying the following demands:

$$H_R = H_R^\dagger = H^t \qquad\qquad P(H_R) = P(U H_R U^{-1}) \tag{2.7}$$

The first equation of (2.7) implies time reversal of the system, the latter should hold for any orthogonal basis transformation $U^{-1} = U^t$ and guaranties the independence of the probability P from the choice of the basis. By using these properties one can show that the probability distribution for the spacings of the eigenvalues in the ensemble follow a Wigner-Dyson distribution:

$$P_{\text{WD}}(s) = \frac{s\pi}{2} e^{-\frac{\pi}{4}s^2} \tag{2.8}$$

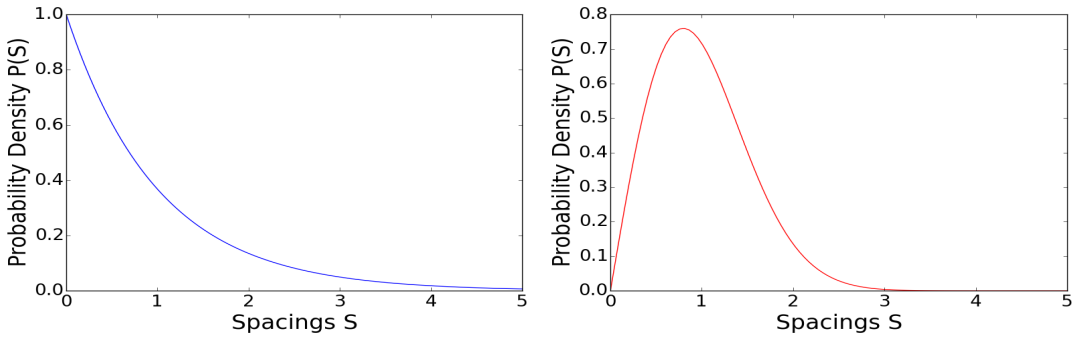

(a) Poisson statistics (2.6) (regular)

(b) Wigner-Dyson statistics (2.8) (chaotic)

Figure 2.1: Predicted Spectral densities

The main difference between those densities is that in a regular system the maximum lies at zero reflected in a so-called clustering of the energy levels, while in the latter case the density vanishes at zero resulting in level repulsion [10]. The maximum of the second distribution is instead at one due to the unfolding.

Alternatively, as recently has been shown [12, 13, 14], it is possible to analyze the probability density of the dimensionless variable r_i defined by the ratio of adjoining spacings s_i, s_{i+1}:

$$0 \leq r_i := \frac{min(s_i, s_{i+1})}{max(s_i, s_{i+1})} \leq 1 \tag{2.9}$$

The crucial advantage is that there is no need for an unfolding, because this ratio is free of the global trend of the spectrum. By assuming that s_i and s_{i+1} are independent random variables obeying (2.6) or (2.8) respectively, one can derive the following densities:

$$P_{reg}(r) = \frac{2}{(1+r)^2} \qquad P_{chaos}(r) \approx \frac{27}{4}\frac{(r+r^2)}{(1+r+r^2)^{5/2}} \tag{2.10}$$

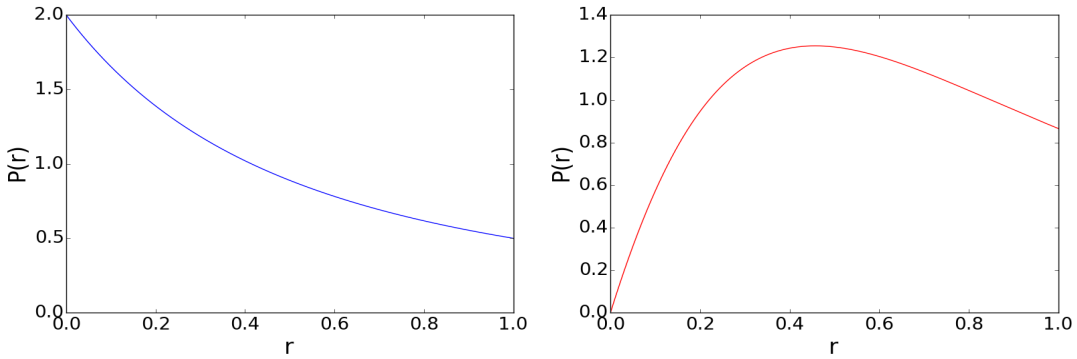

(a) regular

(b) chaotic

Figure 2.2: Probability Density P(r) according to (2.10)

While the latter two methods only characterize the nearest neighbor statistics in the spectrum, it is also possible to examine the range L of these correlations, by evaluation of the quadratic deviation of the unfolded spectral density ρ from its mean $\overline{\rho}$:

$$\Sigma^2(L) = \left\langle \left(\int_{\tilde{E}}^{\tilde{E}+L} \mathrm{d}E\big(\rho(E) - \overline{\rho}(E)\big) \right)^2 \right\rangle_{\tilde{E}} \overset{(*)}{=} \left\langle \left(\int_{\tilde{E}}^{\tilde{E}+L} \rho(E)\mathrm{d}E - L \right)^2 \right\rangle_{\tilde{E}} \tag{2.11}$$

where $\langle \cdot | \cdot \rangle_{\tilde{E}}$ denotes an average such that the interval runs over the whole spectral range and $(*)$ holds because $\overline{\varrho}(E) = 1$ due to the unfolding. Again, the results can be compared to RMT-predictions to identify chaotic or regular behavior:

$$\Sigma_{regular}(L) = L \tag{2.12}$$

$$\Sigma_{chaotic}(L) = \frac{2}{\pi^2}\big(\ln(2\pi L) + \gamma + 1 - \frac{\pi^2}{8}\big) + \mathcal{O}(\frac{1}{L}) \tag{2.13}$$

In the second equation the Euler constant $\gamma \approx 0,57722$ is appearing.
Generally, one will find accordance to these predictions from a not too small value L (so that the $\mathcal{O}(\frac{1}{L})$-term is negligible) up to some system-dependent value.

As already stated, the symmetries of the system represent a redundancy in the description and each of the symmetrized subsystems evolves in time decoupled from the others. Such a statistic analysis thus only makes sense for each subsystem separately, otherwise the mixing of several blocks leads to the fact that the nearest neighbor spacings we compute do not necessarily belong to the same sub-spectrum.

The relevant symmetries for our problem are the discrete permutations of the occupation numbers:

$$P\,|n_1, \cdots, n_L\rangle = |n_{i_1}, \cdots, n_{i_L}\rangle \tag{2.14}$$

The reason for this is that the second quantization formalism already takes into consideration the indistinguishability of the particles and the tight-binding approximation in the Bose-Hubbard model guaranties the particles to be located in one of L sites.

2.4 Numerical Methods

Some of the effects we want to observe in the latter, will only arise when N is adequately high. Because the dimensionality S increases fast with N, our possibility to integrate the emerging systems of ODEs efficiently is essential for the results.

2.4.1 Quantum Jump Method

The time evolution of a state vector $|\psi\rangle$ corresponds to the integration of D coupled ODEs, while the evolution of the density matrix ϱ requires integration of D^2 ODEs. For later purposes D will be in the order of 10^3, so that the numerical effort in the second case is 3 orders of magnitude higher.

The density matrix ϱ can be written in the following form:

$$\varrho = \sum_\alpha p_\alpha |\psi_\alpha\rangle \langle\psi_\alpha| \qquad \left(\sum_\alpha p_\alpha = 1\right) \tag{2.15}$$

This allows the interpretation of ϱ as an ensemble of $|\psi_\alpha\rangle$ distributed with the classical probabilities p_α. Keeping this in mind, it is not surprising that it is possible to consider the time evolution of ϱ as a statistic process, where each realization corresponds to a so-called quantum trajectory $\left|\psi^{(i)}(t)\right\rangle$. Instead of propagating the density matrix directly in time, we can calculate a sufficiently high number of trajectories separately to estimate the process through an ensemble average.

For concrete application this means one has to calculate each quantum trajectory independently and then approximate the desired expectation values of observables by averaging over the realizations $\left|\psi^{(i)}(t)\right\rangle$.

$$\left\langle \hat{O} \right\rangle (t) = \mathrm{Tr}\Big(\hat{O}\varrho(t)\Big) = \lim_{R\to\infty} \frac{1}{R} \sum_{i=1}^{R} \left\langle \psi^{(i)}(t)\middle|\hat{O}\middle|\psi^{(i)}(t)\right\rangle \tag{2.16}$$

We can give an estimation of the statistical error resulting from the finite number of realizations R by calculating the standard deviation from the average. Taking this into account, we are able to choose R accordingly to the desired precision:

$$\sigma^2(R,t) = \frac{1}{R(R-1)} \sum_{i=1}^{R} \left(\hat{O}^{(i)}(t) - \overline{O}(t)\right)^2 \sim \frac{1}{R} \tag{2.17}$$

In all our applications the propagation of $\left|\psi^{(i)}\right\rangle$ will be a peace-wise deterministic process, where the development of the state vector is caused by an effective Hamiltonian

$$H_{\text{eff}} = H - \frac{i}{2} \sum_i \gamma_i A_i A_i^\dagger \tag{2.18}$$

interrupted by sudden quantum jumps[2] when the norm of $\left|\psi^{(i)}\right\rangle$ reaches a random value $\eta \in [0,1]$. This artificial reduction of the norm only serves to determine the exact moment of the next jump and will be removed afterwards by renormalizing the state. Even though we have to iterate this process, we can easily parallelize these computations in contrast to the propagation of ϱ where each integration step needs the information of the previous one.
The exact procedure used to generate the trajectories is adapted from [7] and carried out precisely in the appendix (6.4).

[2] induced by the projection with the related Lindblad operator: $|\psi'\rangle = \frac{A_i|\psi\rangle}{\|A_i|\psi\rangle\|}$

2.4.2 Integration of ODEs

As an integrator we decide for the in Python implemented routine Odeint that is an implementation of the Fortran package LSODA [15, 16]. The algorithm dynamically changes between the integration methods Adams and BFD in order to deal with stiff as well as with non-stiff problems.

Another advantage of this integrator is its adaptive step size, maximizing the integration step, under the condition that the error of the calculated solution does not exceed a specified value. On the other hand, this means that the algorithm needs some iterations until the optimal step size is reached.

When using this integrator in the quantum jump method we have to check the norm of $|\psi\rangle$ after appropriate time steps δt. Before starting the procedure we therefore estimate a value for δt such that it is far smaller ($\approx$ 2 orders of magnitude) than the typical time between two quantum jumps given by the inverse rate at which the norm decreases:

$$\delta t << \frac{1}{\langle\psi|\sum_i \gamma_i A_i A_i^\dagger|\psi\rangle} \tag{2.19}$$

This δt gives the points in time for which an output is generated, that allows us to calculate the norm. In between these points the integrator will use a sufficient number of steps to stick to a given error boundary.

The last problem to solve is to avoid calling odeint for only integrating a single step δt alone. On the other hand, we don't know exactly when the next quantum jump is going to happen. All information calculated beyond the time of the jump will have to be discarded. We therefore estimate another step Δt on the basis of the difference of the norm from the value η where the next jump will happen and the rate at which the norm has decreased between the last two time steps. Then we calculate $\{|\psi(t_0+\delta t)\rangle, |\psi(t_0+2\delta t)\rangle, \ldots, |\psi(t_0+\Delta t)\rangle\}$. If the norm reaches the value of η at a certain point in this range, we perform the jump and use this time as starting-point for the next calculation, otherwise the last point is used. This procedure is repeated until a final value t_{end} is reached.

Chapter 3

Analysis of the Closed System

3.1 Construction of our Model

Our goal in the following is to find an appropriate model to simulate numerically the refilling dynamics in a 1-D-Bose-Hubbard chain realized with ultra-cold atoms in an optical lattice.
The experimental setup [6] we refer to, consists of a lattice with a number of sites L in the order $20 - 100$ and an average particle number per site of $\overline{n} \approx 600$.
The pot in the middle gets emptied to a particle number $\sim 10\%$ of its original value and the occupation number in the central site is observed until the average filling is reached again.

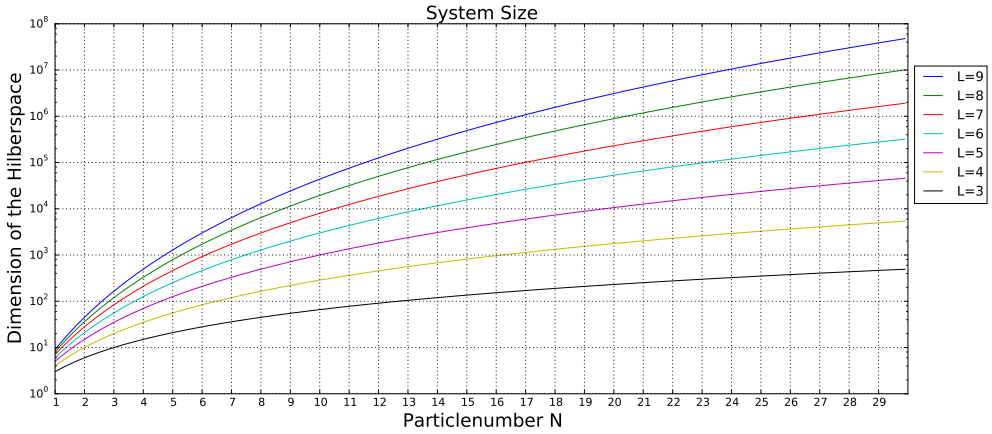

Figure 3.1: Dimensionality D as function of particle number N for various numbers of pots L (eq. 2.4)

As the above figure indicates, it is far beyond our reach to simulate this system directly[1]. Instead, we will restrict ourselves to the emptied pot and its nearest neighbors. One should be aware that this approximation does alter the temporal progress of the occupation numbers of the exterior sites:
While in the experiment they can be assumed to be constant due to the high number of involved sites, in our model they will reduce by $\frac{1}{3}$ each since $N = const.$

[1]For example for $L = 5$ and $N = 20$ we would already need more than 7Gb of RAM only to save every entry of the Hamiltonian

The fact that we can observe a refilling process at all is remarkable. As already shown in [17], a high difference in the occupation number of connected sites leads to a suppression of the tunneling and a so called self trapped state. This can be understood as a consequence of energy conservation:
By comparison of the total energy of the states $\left|\frac{N}{2}, 0, \frac{N}{2}\right\rangle$ and $\left|(\frac{N}{2}-1), 1, \frac{N}{2}\right\rangle$ (N even) one finds a difference of:

$$\Delta E = \frac{U}{2}\left(\tfrac{N}{2}(\tfrac{N}{2}-1) - (\tfrac{N}{2}-1)(\tfrac{N}{2}-2))\right) = U(\tfrac{N}{2}-1) \tag{3.1}$$

With increasing N this difference gets larger and the two states get out of resonance. According to [6] the 2-dimensional spacial extend of the lattice sites is the reason for a nonzero effective tunneling coefficient.

Even though the trapping frequency along the Bose-Hubbard chain is sufficiently high to assume that only the lowest energy band is occupied, the one perpendicular to it is far smaller. This makes it possible for a particle in one of the full sites to tunnel into a radial excited state in the central site.
Our attempt to include this circumstance into our discussion, is to split up the central site in two virtual sites: one with a potential $\epsilon > 0$[3] and one with $\epsilon = 0$. Considering that the eigenfunctions of the harmonic oscillator form an orthonormal basis, $\langle\psi^i|\psi^j\rangle = \delta_{ij}$ it is reasonable to set $J = 0$ for the unitary transition between excited and ground state, while the tunneling coefficient from the adjoining cites in the excited state should be corrected by factor $0 < \eta < 1$ corresponding to a smaller overlap between the wave functions.

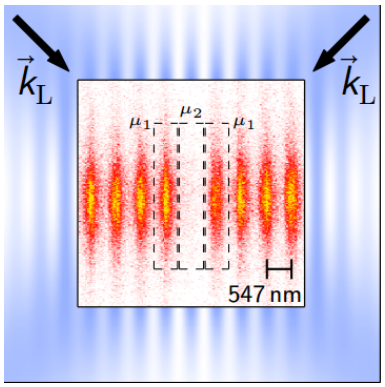

Figure 3.2: Experimental configuration[2]

Leaving the model as it is, the time evolution would be unitary and thus reversible. After all this is totally contrary to the experimental observations, where the system tends to a state with equal filling in each site.
To model this we will suggest different Lindblad operators corresponding to environmental interactions that will prohibit the system from oscillating and destroy coherence.
Their physical origin lies in thermal collisions with the surrounding gas or with the laser. In conclusion our Hamiltonian is based on a system of the following kind:

[2]taken from [6] with kind permission of Sandro Wimberger
[3]thus being referred to as 'excited state'

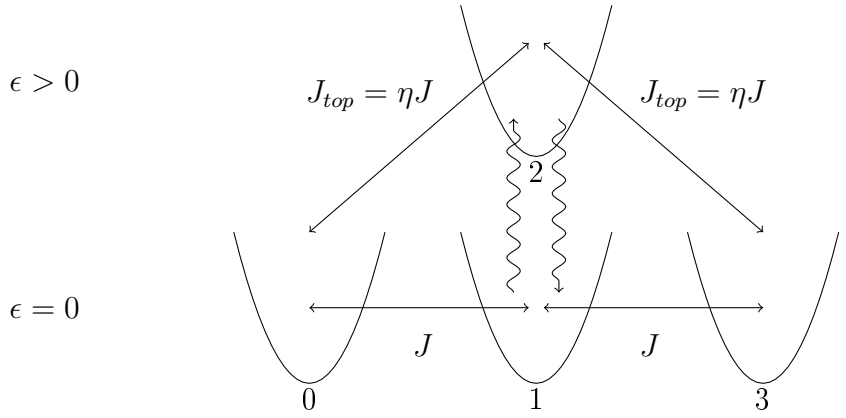

Figure 3.3: model for the refilling dynamics

An excited oscillator state is introduced as a virtual pot with a potential $\epsilon > 0$. The curved lines indicate a not yet specified dissipative process.

3.2 Chaos and Regularity

According to our latest considerations all further calculations will base on a 2-D-Bose-Hubbard model with the number of sites $L = 4$.
We take this as an impetus for a general spectral analysis of the Hamiltonians corresponding to the following 3 graphs. For a systematic approach to the analysis of a wider range of systems, we would like to refer the interested reader to [18]. The first one simply arises from our model in the limit of $\epsilon \to 0; \eta \to 1$, in the

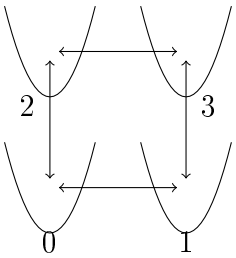

(a) Fig. 3.3 with $\epsilon \to 0; \eta \to 1$

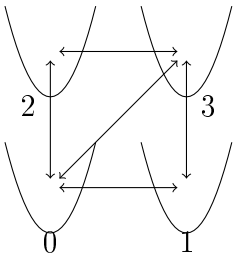

(b) periodic boundary conditions

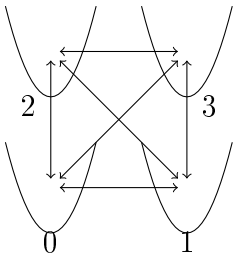

(c) completely connected graph(CCG)

Figure 3.4: Systems of interest

second one we have imposed periodic boundary conditions connecting the sites number 0 and 3. Although there is not a direct connection between system (c) and our model because we explicitly demand the coupling between site 1 and 2 to vanish, we will find a trend in the behavior of such systems for an increasing number of couplings, which is why it will be an interesting case.

The Hamilton operator depends on two parameters U and J, but by writing

$$H = J \cdot \frac{H}{J} = J\left(\frac{U}{2J}\sum_{i=1}^{L}\hat{n}_i(\hat{n}_i - 1) - \sum_{couplings(i,j)}(a_i^\dagger a_j + a_j^\dagger a_i)\right) \tag{3.2}$$

one easily can see that J gives the time scale of the dynamic, while the qualitative behavior only depends on the ration $\frac{U}{2J}$. We therefore set $J \equiv \frac{1}{\hbar}$ measuring time in units of $\frac{J}{\hbar}$ and choose the control parameter of the system to be U.
The symmetries we chose to achieve block structure of our Hamiltonians are the two permutations P_{12} and P_{03} defined by:

$$P_{ij}\,|n_1, \ldots, n_i, \ldots, n_j, \ldots, n_L\rangle := |n_1, \ldots, n_j, \ldots, n_i, \ldots, n_L\rangle \tag{3.3}$$

Obviously the symmetries commute and both fulfill $P_{12}^2 = P_{03}^2 = \mathbb{1}$ which implies that the eigenvalues are $\lambda_{12} = \lambda_{03} = \pm 1$.

For every permutation P there exists an $n \in \mathbb{N}$ such that:

$$P^n = \mathbb{1}\ (\Rightarrow \lambda^n = 1) \tag{3.4}$$

Only using this general property, it is possible to give a way to construct an normalized basis $\{|e_\lambda\rangle\}$ from the vectors of the Fock basis $\{|e\rangle\}$, where each $|e_\lambda\rangle$ is an eigenvector of P:[4]

$$|e'_\lambda\rangle = \sum_{i=0}^{n-1}\lambda^{-i}P^i\,|e\rangle \qquad |e_\lambda\rangle = \frac{|e'_\lambda\rangle}{\|e'_\lambda\|} \tag{3.5}$$

Because then:

$$P\,|e_\lambda\rangle = \sum_{i=0}^{n-1}\lambda^{-i}P^{i+1}\,|e\rangle = \sum_{i=1}^{n}\lambda^{-(i-1)}P^i\,|e\rangle$$

$$= \lambda\left(\sum_{i=1}^{n-1}\lambda^{-i}P^i + \underbrace{\lambda^{-n}P^n}_{=\lambda^{-0}P^0}\right)|e\rangle = \lambda\,|e_\lambda\rangle$$

If two symmetries commute, this procedure can be repeated to get eigenvectors of both symmetries.
As described in section (2.3) we can now apply a basis transformation to this new basis, which we first ordered by the eigenvalues of P_{03} then P_{12}. In the following we use the notation $H_{\lambda_{03},\lambda_{12}}$ referring to the block of the transformed Hamiltonian that corresponds to the eigenvalues $\lambda_{03}, \lambda_{12}$. We focus on the analysis of $H_{-1,+1}$ because in 2 of the 3 cases we consider, the blocks to equal eigenvalues can be decomposed further by making use of the symmetry $P_{20} \cdot P_{31}$.

As a first indicator whether our systems behave regular or chaotic, we vary our control parameter U in the interval [0.01,100] in logarithmic steps and use a χ^2-test to compare the unfolded spacings to the RMT predictions.

[4] to guaranty linear independence, identical vectors obtained through this constructions have to be omitted

Therefore we have to calculate the eigenvalues of $H_{-1,+1}(U)$ numerically and unfold the spacings of the spectrum by the following procedure [3]:

(i) We order the spectrum $\{E_i\}$

(ii) $E_i' = \frac{E_i - E_{min}}{E_{max} - E_{min}} \rightarrow E_i' \in [0,1]$

(iii) Spacings: $S_i = E_{i+i} - E_i$

(iv) unfolded Spacings: $S_i' = \frac{S_i}{\langle S_i \rangle_{nn}} = \frac{2nn+1}{E'_{i+nn+1} - E'_{i-nn}} S_i$

with the free parameter nn giving the number of spacings for a local average $\langle S_i \rangle_{nn}$. To compare this discrete distribution to the densities given in (2.6) and (2.8) we display our data in a histogram with N_{bins} bins. Then we calculate the difference of the fraction of spacings found in the interval of the i-th bin $I_i = [a_i, b_i]$ and the one given by $\int_{a_i}^{b_i} P(S)\mathrm{d}S =: N_i^{expected}$.
As a measure of deviation from the chaotic or regular behavior we define:

$$\chi^2(U, N_{bins}) = \sum_{i=1}^{N_{bins}} \frac{(N_i^{expected} - N_i^{spectrum})^2}{N_i^{expected}} \tag{3.6}$$

$$\chi^2_{\log}(U) := \min_{N_{bins}} \left\{ \log\left(\frac{\chi^2(N_{bins}, U)}{N_{bins} - 1} \right) \right\} \tag{3.7}$$

where the latter is finally independent of the number of bins. Here one has to be careful with setting a range of N_{bins} to vary over. A choice of $N_{bins} = 1$ is not a reasonable one but will give a very small deviation from both the chaotic and the regular case because single interval contains all spacings.
While in Fig.(3.5)(a) $\chi^2_{\log,\mathrm{chaos}}$ stays smaller than zero for most values over two orders of magnitude $(10^{-2} - 10^{0})$ this behavior can only be observed over one order $(10^{-1} - 10^{0})$ in (b) and in (c) one can not even identify a significant minimum of the curve. Additionally values of the minima increase from (a) $\rightarrow$ (c).

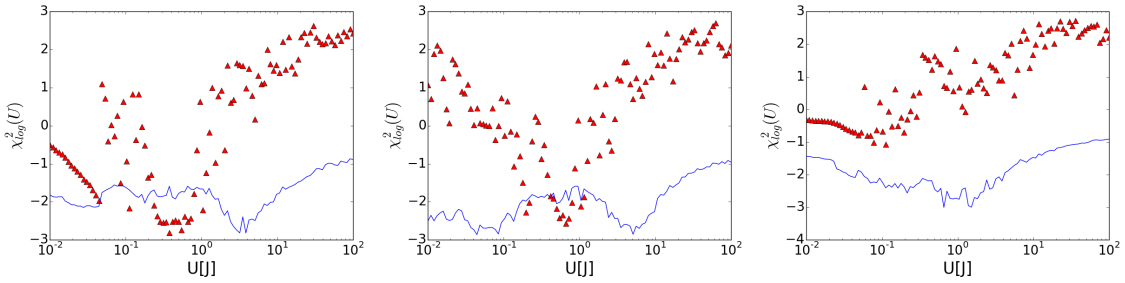

(a) no diagonal coupling (b) one diagonal coupling (c) two diag. couplings (CCG)

Figure 3.5: $\chi^2_{\log}(U)$

The deviation from the chaotic case (red triangles) and from the integrable system (blue line). $15 \leq N_{bins} \leq 35$ and $nn = 5$ in the unfolding; particle number $N = 20$

We only presented the χ^2_{log}-plots for $N = 20$, but we find the same qualitative behavior for the whole tested range of $10 \leq N \leq 30$.

For of the cases with one diagonal coupling where $\chi^2_{\log}$ gets minimal, we exemplarily display the distribution of the unfolded spacings and perform further analysis as introduced in section (2.3).

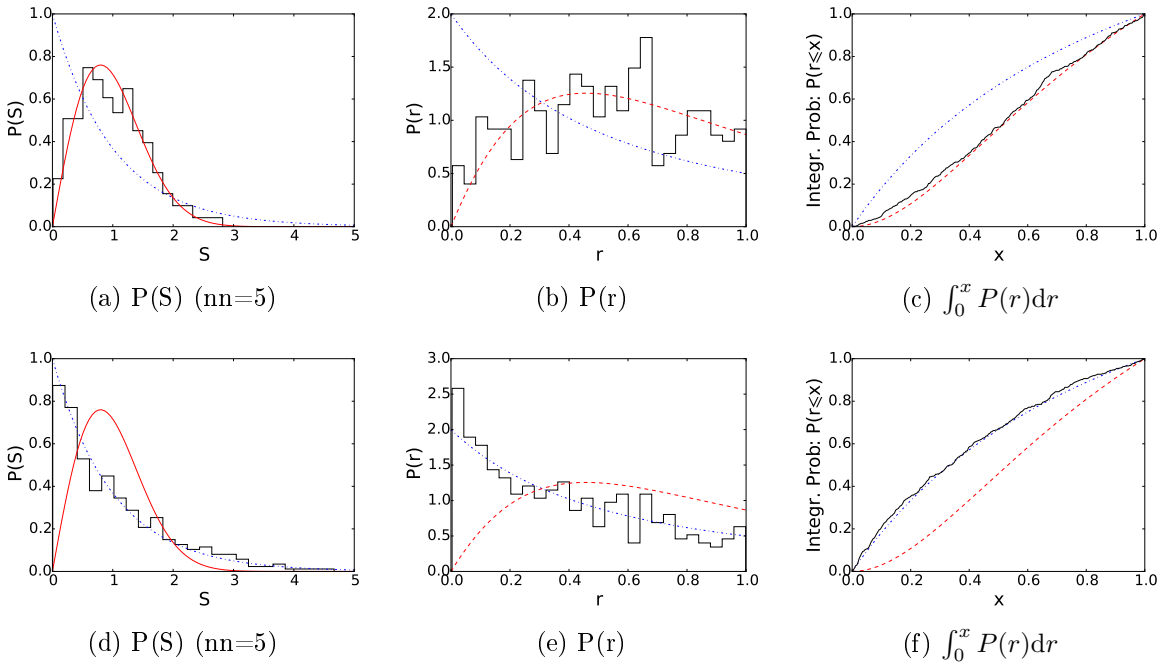

(a) P(S) (nn=5) (b) P(r) (c) $\int_0^x P(r)\mathrm{d}r$

(d) P(S) (nn=5) (e) P(r) (f) $\int_0^x P(r)\mathrm{d}r$

Figure 3.6: Statistics for one diagonal coupling; N=20

Chaotic case ($U = 0.657$) in the top row; regular ($U = 0.0443$) in the bottom. Data obtained from spectral analysis (black) vs predictions for chaotic (red) and regular (blue) systems

Our data fits well the predictions for both of the methods. Though the statistical fluctuations around the theoretical curves in (3.6)(b) and (c) are not small, the integrated density shows good concordance, since it is statistically more stable.

So far we only analyzed nearest neighbor statistics. In the next step we will characterize the range of correlations in the spectrum by applying a Σ^2-test. While fig. (3.7) (b) shows the expected behavior, (a) only coincides with the linear curve over a tiny interval.
Although our choice of $nn = 5$ provided good results in the nearest neighbor statistics, this range is too short for optimal results in the long range correlation.

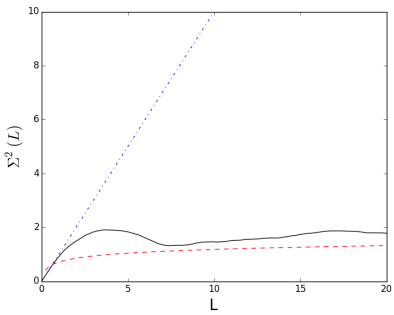

(a) N=20; regular; nn=5

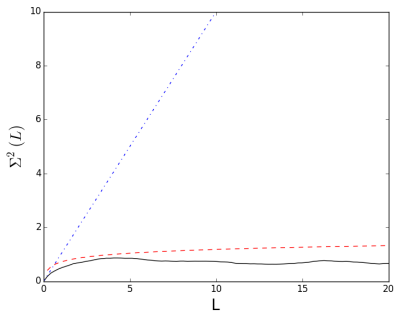

(b) N=20; chaotic; nn=5

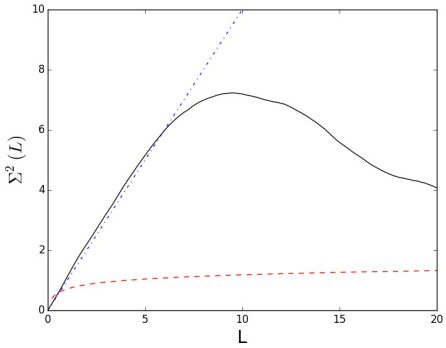

(c) N=20; regular; nn=10

Figure 3.7: Σ^2-test (one diagonal coupling)

Predictions for a regular (blue) and a chaotic (red) system. Obtained data (black). Accordance with theoretical predictions gets better for the regular system (a) $\rightarrow$ (c).

For the CCG system, even the most chaotic case fits far better to the predictions for regular systems, so that we conclude it to behave regular over the whole parameter range. These observations are in good agreement to the results of [19] where it could be shown that CCG systems can at least in the limit $L \rightarrow \infty$ be described by an infinitely ranged mean field approximation. Our data indicates that not only this extreme case shows greater regularity, but that even adding single couplings could serve as a method to regularize a system.

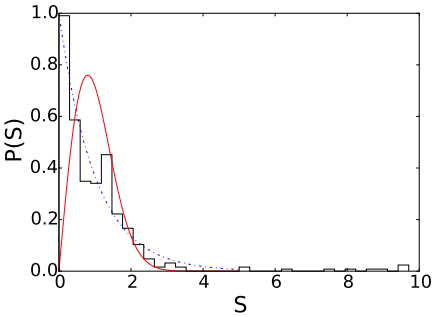

(a) P(S)

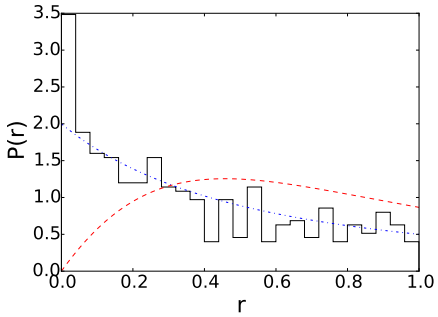

(b) P(r)

Figure 3.8: CCG U=0.112 (where least regularity is expected from fig. (3.5)(c))

Normalized histogram of the obtained data (step); theoretical predictions for the chaotic(green) and regular(blue) case

3.3 Dynamics and System Parameters

Our model system involves the unknown parameters (N, U, η, ϵ) and for every dissipative process we add, we have to specify another rate γ_i. This high amount of parameters makes an analysis of the unitary dynamics in advance inevitable. In this section, we will set $\eta = 1$ and examine the behavior of the system when we vary ϵ for given N and U. More precisely we are interested in the average occupation number of the excited state $\overline{n}_{ex}$ giving a measure how resonant the excited state is with the pots of high filling.

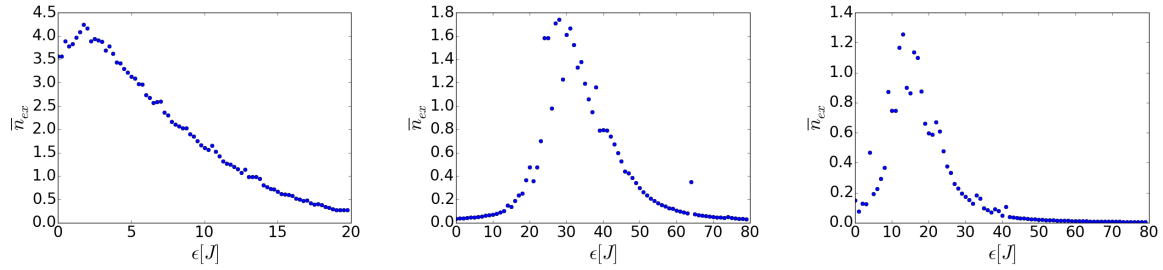

(a) $N = 17$; $U = 1$ (b) $N = 17$; $U = 5$ (c) $N = 10$; $U = 5$

Figure 3.9: Average filling in the excited state $\overline{n}_{ex}$ as a function of ϵ

The filling shows peak-structure around a value ϵ_{max} that increases with N and U.

Fig. (3.9) displays $\overline{n}_{ex}$ averaged over $t = 100\frac{\hbar}{J}$[5]. We can observe a peak in each of the curves. The value ϵ_{max} where best resonance is achieved is displayed as a function of N for various values U in fig. (3.10).

As the graphs show, we find approximately linear behavior. In order to compare this trend to eq. (3.1) for the energy difference that causes the self-trapping, we fit linear curves of the following form:

$$\epsilon_{max} = C(\frac{N}{2} - 1) - c_{shift} \qquad (3.8)$$

with the slope $\frac{C}{2}$ and a constant c_{shift}, that is caused by the small size of the system, allowing the excited state to stay in resonance even after it is already occupied by one particle. For $U > 1$ the values of C coincide within their 3-σ-range with U. We therefore conclude that introducing an on-site potential ϵ is indeed the right approach to dissolve self-trapping and a value according to (3.1) is the right choice if a small filling in the excited state is desired.

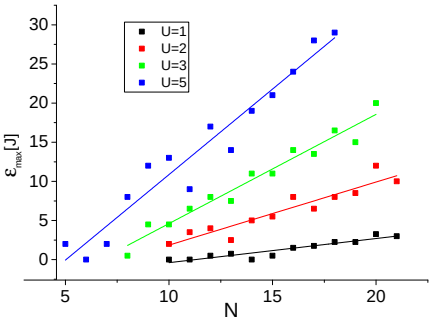

Figure 3.10: Values ϵ_{max} where best resonance is found

U[J]	C	c_{shift}
1	0.62 ± 0.07	2.86 ± 0.55
2	1.61 ± 0.18	4.59 ± 1.47
3	2.79 ± 0.17	6.56 ± 1.28
5	4.37 ± 0.3	6.61 ± 1.92

[5]initial state: $|N, 0, 0, N\rangle$ (N even) or $\frac{1}{\sqrt{2}}(|N, 0, 0, N+1\rangle + |N+1, 0, 0, N\rangle)$ (N odd)

Chapter 4

Interactions with the Environment

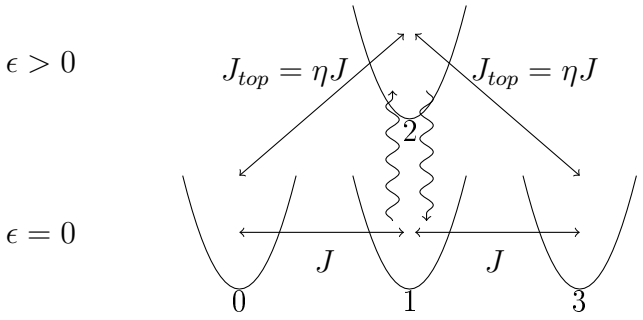

In the following we always consider a system with $N = 20$, and an initial state $|10, 0, 0, 10\rangle$. According to the considerations of sec. (3.3) we will choose $\epsilon = U(\frac{N}{2} - 1) = 18$. Together with $\eta = 0.3$ this will result in the following unitary dynamics:

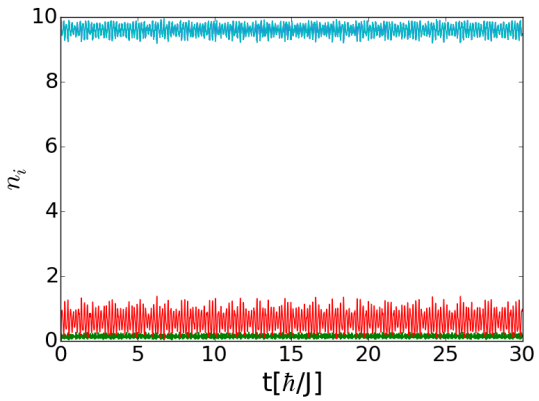

Figure 4.1: Unitary Dynamics

Occupation number in the exterior (blue) sites, the excited (red) and the ground state (green)

With this choice of parameters, we get a self trapped state, only with a small oscillation of amplitude $\Delta n < 1$ in the excited state and the half of this value in the exterior sites. The filling of the ground state is negligible, guaranteeing that the cause of the refilling are environmental interactions.
After using the symmetry P_{03} to obtain block form of the Hamiltonian, we will observe the dynamics of the symmetry-reduced subsystem given through Master Equations with the 3 following Liovillians. The time evolution is performed by use of the quantum jump method.

4.1 Global Noise

In a first, naive approach we assume, that the decoherence is induced by noise, acting on each pot with the same rate κ. The corresponding Lindblad operators for such a process are the particle number operators of the sites $\{n_i\}$:

$$\mathcal{L}[\varrho] = \frac{\kappa}{2} \sum_{i=0}^{3} (2n_i \varrho n_i^\dagger - n_i^\dagger n_i \varrho - \varrho n_i^\dagger n_i) \tag{4.1}$$

The time step δt at which the norm of our trajectories $\|\psi^{(i)}\|$ is evaluated has to be much smaller than the typical time between 2 jumps, meaning:

$$\frac{1}{k \left\langle \sum_{i=0}^{3} n_i n_i^\dagger \right\rangle} \overset{\substack{n_i^\dagger = n_i \\ n_i \leq 10}}{\geq} \frac{1}{k \cdot 2 \cdot 10^2} = \frac{1}{200\kappa} >> \delta t \tag{4.2}$$

Following this, we calculate the time evolution for a range of parameters.

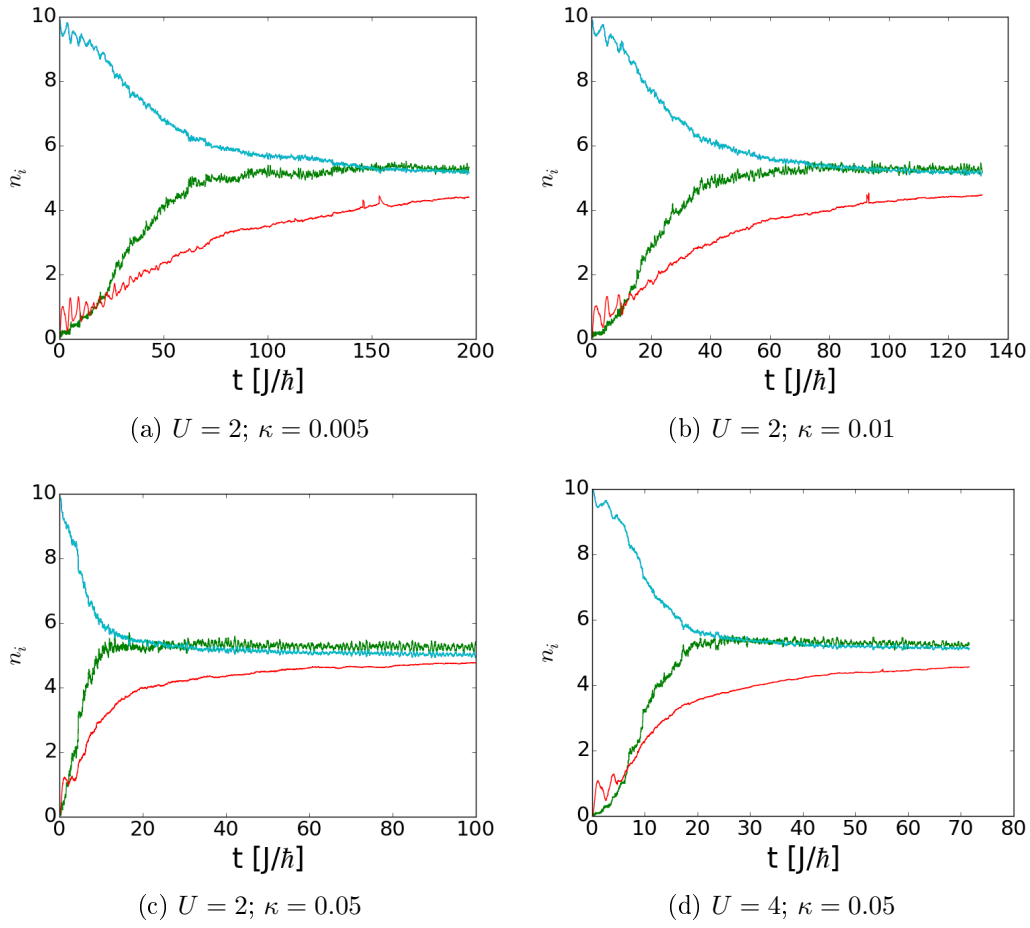

(a) $U = 2$; $\kappa = 0.005$

(b) $U = 2$; $\kappa = 0.01$

(c) $U = 2$; $\kappa = 0.05$

(d) $U = 4$; $\kappa = 0.05$

Figure 4.2: Global noise with parameter κ for $U = 2J$ and $U = 4J$

Filling of the exterior sites (blue), the excited state (red) and the ground state (green).

Even though we can observe the expected S-shape of the filling in ground state in each of fig. 4.2 (a-c) this model leads to an increasing particle number in the excited state as well. The equilibrium value of n_{ex} is only a little smaller than the one of the sites with $\epsilon = 0$. This difference in the stationary state even decreases with rising κ. This can be understood in the following way: A greater value of κ corresponds to a higher collision rate and therefore a higher temperature in the thermal cloud surrounding the Bose-Einstein condensate. Though the excited state has an on-site potential and is therefore energetically unfavorable, the system tends to a more disordered process for rising κ.
In the experiment [6] one can clearly observe a decreasing of the width of the condensate in the central site over time. Because the spread of an excited oscillator state is larger than the one of the ground state, we therefore would expect the exact opposite of what is visible in 4.2.

4.2 Local Noise for the Excited State

This approach is similar to the previous, but because we identify the pot with an excited oscillator state, this time we take into account that such a state has to have a far wider spreading and therefore offers the thermal cloud surrounding the condensate a bigger target for collisions.
By assuming that these collisions are the dominant factor, we neglect noise terms for the other pots and apply a high collision-rate κ in the excited state. The resulting Liovillian then is:

$$\mathcal{L}[\varrho] = \frac{\kappa}{2}(2n_2\varrho n_2^\dagger - n_2^\dagger n_2\varrho - \varrho n_2^\dagger n_2) \tag{4.3}$$

where the time step of the quantum jump method δt has to obey:

$$\frac{1}{k\left\langle n_{ex}n_{ex}^\dagger\right\rangle} \underset{n_{ex}\leq 2}{\overset{n_i^\dagger = n_i}{\geq}} \frac{1}{k\cdot 2^2} = \frac{1}{4\kappa} >> \delta t \tag{4.4}$$

Fig. 4.3 shows the development of the particle numbers over time. The shape of the curve coincides very well with the results of the experiment: As expected the excited state gets emptied and the filling of the ground state increases in an S-shaped curve. The problem is, that this process happens on a time scale approximately one order of magnitude larger than the experimental refilling.

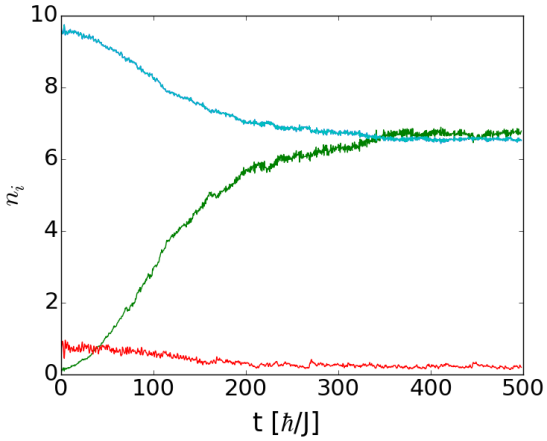

Figure 4.3: $U = 2$; $\kappa = 0.5$

One could think, that a higher value of kappa could accelerate this process but as Fig.(4.4) shows, a higher value of kappa results in a larger slope in the first part of $n_{ground}(t)$, but also the occupation number of the excited state decreases faster. This effectively reduces the jump rate again and in total we get an even larger refilling time.

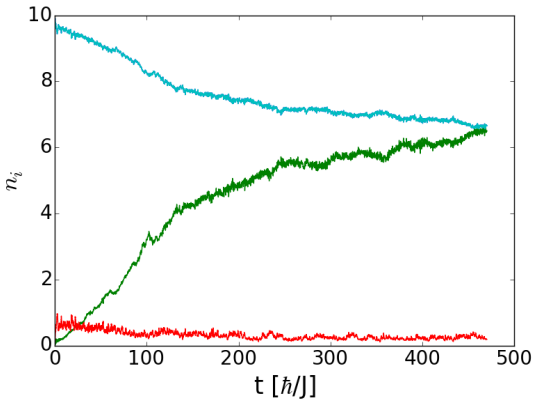

Figure 4.4: $U = 2$; $\kappa = 1$

Filling of the exterior sites (blue), the excited state (red) and the ground state (green). A higher κ results in a faster rise of n_{ground} first, after a short time it decreases such that in total the refilling time gets even larger.

Although with this type of process we can match the course of the refilling, it is not possible to match the time scale as well.

4.3 Excitation and Relaxation

This time we consider two contra-acting processes that take place simultaneously and will lead to a dynamic equilibrium. The operator $A_\uparrow = a_1 a_2^\dagger$ represents the excitation of a particle in the ground state, by receiving energy through a collision with a particle in the cloud and $A_\downarrow$ represents the contrary process. Their form is the same as the part in the Hamiltonian responsible for the tunneling $J_{ij} a_i a_j^\dagger$, but we explicitly do not demand $\gamma_\uparrow = \gamma_\downarrow$ contrary to the Hamiltonian tunneling. Moreover - in accordance with the underlying model - we allow the total energy to change under excitation and relaxation.

$$A_\uparrow = a_1 a_2^\dagger;\ A_\downarrow = a_2 a_1^\dagger;\ A_\uparrow^\dagger = A_\downarrow$$

$$\mathcal{L}[\varrho] = \frac{\gamma_\downarrow}{2}(2A_\downarrow \varrho A_\uparrow - A_\uparrow A_\downarrow \varrho - \varrho A_\uparrow A_\downarrow) + \frac{\gamma_\uparrow}{2}(2A_\uparrow \varrho A_\downarrow - A_\downarrow A_\uparrow \varrho - \varrho A_\downarrow A_\uparrow) \tag{4.5}$$

and:

$$\frac{1}{\gamma_\uparrow \langle A_\uparrow A_\downarrow \rangle + \gamma_\downarrow \langle A_\downarrow A_\uparrow \rangle} \gtrsim^{1} \frac{1}{(\gamma_\uparrow + \gamma_\downarrow)(n_2+1)n_1} \geq \frac{1}{(\gamma_\uparrow + \gamma_\downarrow)2 \cdot 10} >> \delta t \tag{4.6}$$

As one would expect, the resulting filling in the ground state of the middle pot depends on the relation between the two parameters $\gamma_\uparrow$,$\gamma_\downarrow$, while the refilling time depends on the total rate of jumps occurring and therefore their sum.

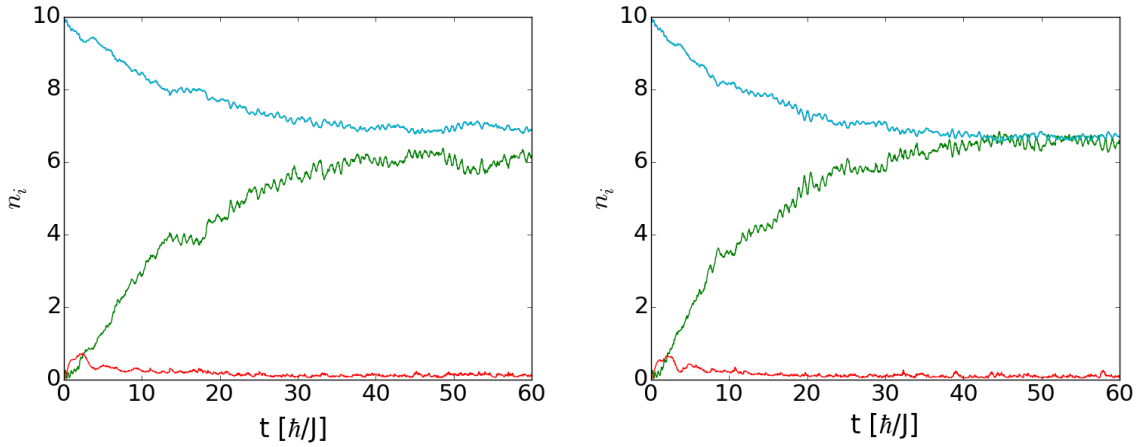

(a) $\gamma_\downarrow = 0.8$; $\gamma_\uparrow = 0.1$

(b) $\gamma_\downarrow = 0.9$; $\gamma_\uparrow = 0.1$

Figure 4.5: Occupation numbers of the different sites as a function of time. Exterior sites (blue), excited state (red) and ground state (green)

[1] $\gamma_\uparrow \langle A_\uparrow A_\downarrow \rangle + \gamma_\downarrow \langle A_\downarrow A_\uparrow \rangle \leq (\gamma_\uparrow + \gamma_\downarrow) \max\{\langle A_\uparrow A_\downarrow \rangle, \langle A_\downarrow A_\uparrow \rangle\}$
$= (\gamma_\uparrow + \gamma_\downarrow) \left\langle a_1^\dagger a_1 a_2 a_2^\dagger \right\rangle \approx (\gamma_\uparrow + \gamma_\downarrow)(n_2+1)n_1$

As a next step we observe which pairs $(\gamma_\uparrow, \gamma_\downarrow)$ will lead to an equal filling in the exterior sites and the ground state of the middle pot. Fig (4.6) shows $\gamma_\uparrow(\gamma_\downarrow)$ such that this condition is fulfilled.

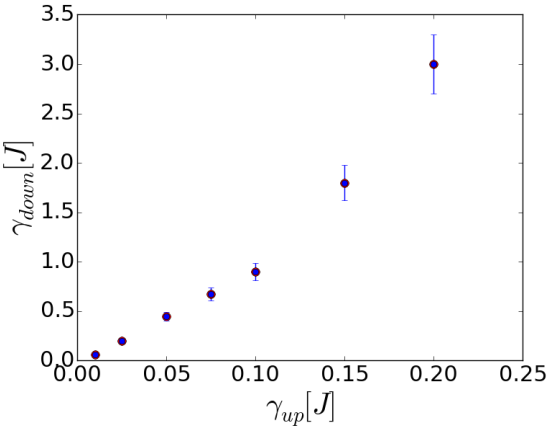

Figure 4.6: Relation between relaxation- and excitation-rate for equal filling outcome

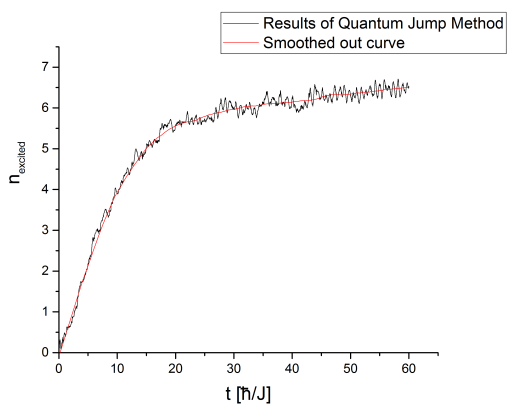

(a) Smoothed out graph ($\gamma_\uparrow = 0.125; \gamma_\downarrow = 1.3$)

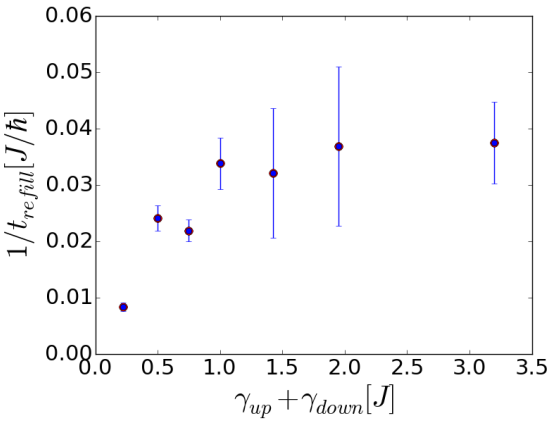

(b) Inverse refilling time

Figure 4.7: Inverse refilling time obtained from smoothed out results $\gamma_\uparrow + \gamma_\downarrow$

Plotted is the inverse of the time where we first reached 90% of the final value for the occupation number of the ground state n_1. The error bars are gained by difference between $1/t$ where 85% filling is reached.

For small values of $\gamma_\uparrow$ we find the almost linear relation $\frac{\gamma_\downarrow}{\gamma_\uparrow} \approx 8$ resulting in an equal filling outcome and refill rate, that rises with the excitation and relaxation rate. This can clearly be distinguished from an other regime, where a far higher relaxation rate is needed to establish an equal filling and inverse refilling time stagnates.

The rate at which jumps are occurring is proportional both to γ and to the number of particles inhibiting the ground and the excited state. When $\gamma_\uparrow$ and $\gamma_\downarrow$ are small,

an increase of their value will enhance the refilling process because the system would not leave the self trapped state only through the unitary dynamics. After a few jumps happened, the self trapping is repealed and the unitary dynamics contribute to the refilling. The induced decoherence in the central site guaranties that constant occupation numbers are reached and suppress oscillations.

But when $\gamma_\uparrow + \gamma_\downarrow$ is in the order of magnitude of the tunneling coefficient $J = 1$, during the refilling a total jump rate is reached that is so high, that the repeatedly performed measurements in form of jumps between the excited and the ground state are so rapid, that no further refilling through the unitary dynamics is experienced.

Similar effects have already been observed for local particle loss processes, where a rising loss rate prohibits particles to tunnel in the lossy site [4, 3] indicating a quantum Zeno effect [20].

Finally, it should be noted that so far in this section we only considered a process between the excited and the ground state to happen. By adding a small noise term for the exterior sites, we can achieve getting a more S-shaped curve (as observed in [6]) fig. (4.8)(b). If κ is chosen too big, the noise dominates the relaxation/excitation process and the equilibrium outcome is different: fig. (4.8)(b).

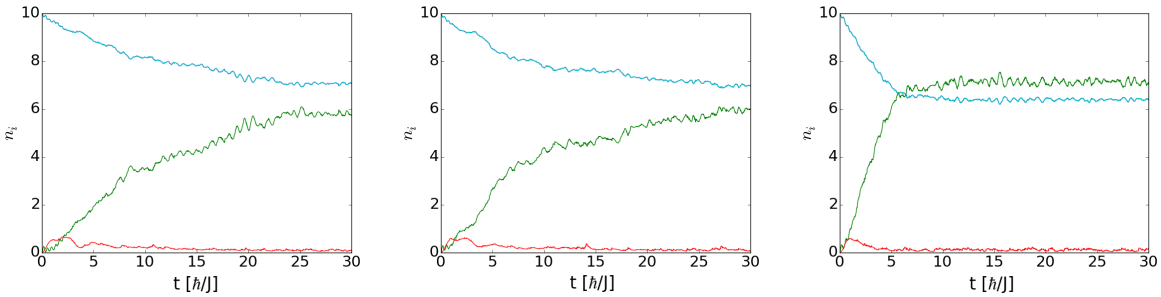

(a) $\kappa = 0$ (b) $\kappa = 0.001$ (c) $\kappa = 0.01$

Figure 4.8: $\gamma_\downarrow = 0.9$; $\gamma_\uparrow = 0.1$; added noise in the exterior sites

Occupation numbers: exterior sites(blue) excited state (red) and ground state (green)

Chapter 5

Conclusion

The analysis of the spectral properties of different 2×2 systems revealed a trend towards regularity for an increasing number of couplings. Due to [19] where it is stated that a completely connected graph can be described by an infinite range mean-field approximation in the limit of the number of sites $L \to \infty$, we expect this to be not a property of the special case $L = 4$ but a more general characteristic which should be investigated - and currently is in [18] - for larger systems as well.

In the second part we considered a model introducing an excited oscillator state as a virtual pot to a one-dimensional Bose-Hubbard chain to simulate the refilling after draining of the central site. We suggested different forms of environmental interactions and their corresponding Liouvillians where the combination of an excitation and a relaxation process turned out to be to most promising assumption. Its main flaw though is, that the rates $\gamma_\uparrow$ for the excitation and $\gamma_\downarrow$ for the relaxation have to be adjusted "by hand" to see a refilling process in the experimentally observed form. For a wide range of parameters the progress of the occupation numbers show qualitatively similar behavior. The filling in equilibrium only depending on the ratio $\frac{\gamma_\downarrow}{\gamma_\uparrow}$ and its timescale on their sum. After exceeding a certain limit we cannot find a matching pair $\frac{\gamma_\downarrow}{\gamma_\uparrow}$ leading to an equilibrium value with equal filling in the ground state of the central site and the exterior sites. Its cause might be the high rates of jumps occurring between excited and ground state prohibiting other particles to tunnel into each of them.
With the appropriate choice of parameters it is possible to describe the systems dynamic at least approximately. On the one hand this is remarkable due to the high order of simplification of our model, on the other hand one might criticize that a number of parameters which have to be tuned to achieve this is too large.

As a next step it would be interesting if one can find a relation between the two rates leading to an equal filling outcome and its dependency of the other system parameters. Considering the fact that the origin of both processes is assumed to lie in thermal collisions with the surrounding particle cloud, it might even be possible to relate the rates via thermodynamical considerations. However getting better accordance with the experimental results may require a different approach involving dynamically changing rates or even other Lindblad operators.

Chapter 6

Appendix

6.1 Spectral Analysis: Symmetry Transformation

```
import numpy as np
import math
from copy import deepcopy
from general import svtxt

def f1(x): #≡ P_03
    tm=np.zeros([4,4],dtype=int)
    tm[0][3]=1
    tm[1][1]=1
    tm[2][2]=1
    tm[3][0]=1
    return list(np.dot(tm,x))

def f2(x): #≡ P_12
    tm=np.zeros([4,4],dtype=int)
    tm[0][0]=1
    tm[1][2]=1
    tm[2][1]=1
    tm[3][3]=1
    return list(np.dot(tm,x))

def order(basis,f): #constructs
    S=len(basis)
    L=len(basis[0])
    result=[[],[]]
    b=list(deepcopy(basis))
    for x in b:
        if f(x)==x:
            result[0].append([x])
        else:
            result[0].append([x,f(x)])
            result[1].append([x,f(x)])
            b.remove(f(x))
    return result

def reorder(ordered,f):
    S=len(ordered)
    L=len(ordered[0])
    result=[[[],[]],[[],[]]]
    b=list(deepcopy(ordered))
    for i in range(2):
        for x in b[i]:
            if f(x[0])==x[0]:
                result[i][0].append(x)
            else:
                result[i][0].append(x+[f(z) for z in x])
                result[i][1].append(x+[f(z) for z in x])
                try:b[i].remove([f(z) for z in x])
                except:b[i].remove([f(z) for z in x[::-1]])
    return result

def constr(basis,reordered):
```

```
    S=len(basis)
    L=len(basis[0])
    U=np.zeros([S,0])
    structure=[len(x) for y in reordered for x in y]
    for i in range(2):
        for j in range(2):
            for x in reordered[i][j]:
                y=np.zeros([S,1])
                l=len(x)
                if l==4:
                    for n in range(2):
                        for m in range(2):
                            y[basis.index(x[int(n*l/2+m)])]+=(-1)**(j*n+i*m)*0.5
                elif l==2:
                    for n in range(2):
                        y[basis.index(x[n])]+=(-1)**((i+j)*n)/math.sqrt(2)
                elif l==1:
                    y[basis.index(x[0])]+=1
                U=np.hstack((U,y))
    return (U,structure)
```

Listing 6.1: symmetries.py

6.2 Spectral Analysis: Unfolding & χ^2

```
import numpy as np
import matplotlib.pyplot as plt
import math
from scipy.special import pdtr

def unfold(nn,E_list):
    E=E_list
    l=len(E)
    print(E[-1]-E[0])
    E=[(e-E[0])/(E[-1]-E[0]) for e in E ]#E_list->[0,1]
    S=[E[i+1]-E[i] for i in range(l-1)]
    S_n=np.array([(2*nn+1)*S[i]/(E[i+nn+1]-E[i-nn]) for i in range(nn,l-nn-1)])
    return S_n

def chi2(S_n,N_bins):
    x=np.linspace(0,np.amax(S_n),N_bins+1)
    y_regular=1-np.exp(-x)
    y_chaos=1-np.exp(-np.pi/4*x**2)
    value,bins,patches=plt.hist(S_n,bins=x,normed=True,label="spectrum")
    plt.clf()
    mean_c=[y_chaos[i+1]-y_chaos[i] for i in range(N_bins)]
    chi_c=sum((mean_c-value*(x[1]-x[0]))**2/mean_c)
    mean_r=[y_regular[i+1]-y_regular[i] for i in range(N_bins)]
    chi_r=sum((mean_r-value*(x[1]-x[0]))**2/mean_r)
    return [chi_c/(N_bins-1),chi_r/(N_bins-1)]
```

Listing 6.2: unfolding.py

6.3 Construction of the Fock Basis and the Hamiltonian

```
import numpy as np
from math import *
from copy import deepcopy

def build(N,L):
    if L==1:
        return [[N]]
    else:
            M=[[i]+x for i in range(N+1)  for x in build(N-i,L-1)]
    return M

def H_e(N,U,elist,Jlist,jump):#returns hermitean Hamiltonian and
    Jumpoperators
    L=len(elist)
    basis=build(N,L)
    S=len(basis)
    Ham=np.zeros([S,S])
    m=deepcopy(basis)
    #diagonal terms of H
    for i in range(S):
        Ham[i][i]=np.dot(elist,basis[i])+sum([x*(x-1)*U for x in basis[i
    ]])
    #offdiagonal terms of H
    for i in range(0,L-2):#loop over couplings
        for j in range(S):#loop over basis vectors
            if m[j][0]!=0:
                m[j][0]-=1
                m[j][i+1]+=1
                y=basis.index(m[j])
                m[j][0]+=1
                m[j][i+1]-=1
                Ham[j][y]+=-sqrt(m[j][0])*sqrt(m[j][i+1]+1)*Jlist[0][i]
                Ham[y][j]=Ham[j][y]
            if m[j][-1]!=0:
                m[j][-1]-=1
                m[j][i+1]+=1
                y=basis.index(m[j])
                m[j][-1]+=1
                m[j][i+1]-=1
                Ham[j][y]+=-sqrt(m[j][-1])*sqrt(m[j][i+1]+1)*Jlist[-1][i]
                Ham[y][j]=Ham[j][y]
    #Jump-operators
    if jump:
        jump_op=[]
        for i in range(L-3):#loop over jump-operators
            temp=np.zeros([S,S])
            for j in range(S):#loop over basis vectors
                if m[j][i+2]!=0:
                    m[j][i+2]-=1
                    m[j][1]+=1
                    y=basis.index(m[j])
                    m[j][i+2]+=1
                    m[j][1]-=1
                    temp[y][j]+=sqrt(m[j][1]+1)*sqrt(m[j][i+2])
            jump_op.append(temp)
        return Ham,jump_op
    else:
        return Ham
```

Listing 6.3: ham_epsilon.py

6.4 Principle of the Quantum Jump Method

(i) A random $\eta \in [0,1]$ is obtained through a pseudo-random number generator

(ii) ψ gets propagated in time with the effective Hamiltonian $H_{\text{eff}} = H - \frac{i}{2}\sum_i \gamma_i A_i^\dagger A_i$
→ Result: $[\psi(t_i)]$ at the time steps t_i

(iii) calculate $\|\psi(t_i)\|\ \forall t_i$

(iv) if $\|\psi(t_i)\| > \eta$ then the renormalized $\frac{\psi(t_i)}{\|\psi(t_i)\|}$ is saved in a .txt-file.

(v) if $\|\psi(t_i)\| \leq \eta$ then a quantum jump will happen.
→ we decide, which one will happen:

1. for each possible A_i we calculate $p_i = \gamma_i \langle\psi(t_i)|A_i^\dagger A_i|\psi(t_i)\rangle$
2. we calculate the cumulative sum, normalized to unity: $P_i = \frac{\sum_{j=0}^{i} p_i}{\sum_j p_i}$
3. another random variable $r \in [0,1]$ is generated
4. when i is the lowest index where $r \leq P_i$ then jump no. i is executed
5. $\frac{|A_i|\psi(t_i)\rangle}{\||A_i|\psi(t_i)\rangle\|}$ is saved in the .txt and used as initial value in the next time evolution; the following $\psi(t_j), j > i$ are discarded

(vii) if no jump occurred the last value of $\psi(t_i)$ is used as initial value **without** normalizing it

Explicit realization for the initial value "*y0*" a Hamiltonian "H", the list of Lindblad operators "*jump_op*" and the corresponding list of rates "*gamma*":

```
import numpy as np
from scipy.integrate import odeint
import math
from general import wline

def timeevo_QJ(H,y0,tend,dt,dtmax,gamma,jump_op,savepath):

    #derivative function
    def fH(y,t):
        re=np.dot(H,y[l:])-0.5*np.dot(jumpsum,y[:l])
        im=-np.dot(H,y[:l])-0.5*np.dot(jumpsum,y[l:])
        return 2*np.pi*np.hstack((re,im))

    #initialize evolution
    file=open(savepath,mode='w')
    jumplist=[gamma[i]*np.dot(jump_op[i].T,jump_op[i]) for i in range(len
    (gamma))]
    jumpsum=np.sum(jumplist,0)
    l=len(y0)
    tnow=0
    Dt=0
    start=rv(y0)
    norm=1
    ny=np.random.rand(1)[0]


    #time-evolution
    while(tnow<tend):
        #evolution from tnow untill tnow+Dt
```

```
29          step=min(max(np.log(norm/ny)*Dt,10*dt),tend-tnow+dt,dtmax)
30          print("t= %s norm( %s / %s ) start new timeevolution with step %s
      (Dt= %s )" %tuple(np.round([tnow,norm,ny,step,Dt],2)))
31          temp=odeint(fH,start,np.arange(tnow,tnow+step,dt),atol=10**-8,
    rtol=10**-8)[1:]
32          start=temp[-1]
33          for x in temp:
34              #calculate norm of x
35              norm=math.sqrt(np.sum(absv(x)))
36
37              #NO JUMP
38              if norm>ny:
39                  line=np.hstack((tnow,cv(x)/norm))
40                  wline(file,line)
41                  tnow+=dt
42
43
44              #JUMP
45              else:
46                  #which jump?
47                  projection=[np.hstack((np.dot(op,x[:1]),np.dot(op,x[1:]))
    ) for op in jump_op]
48                  p_norm=[np.sqrt(np.sum(absv(projected))) for projected in
      projection]
49                  p=[gamma[i]*p_norm[i] for i in range(len(gamma))]
50                  p=np.cumsum(p)/np.sum(p)
51                  rand=np.random.rand(1)
52                  jump_index=np.where(p>rand)[0][0]
53
54                  #execute jump
55                  print(tnow,"QUANTUM JUMP NR.:",jump_index)
56                  start=projection[jump_index]/p_norm[jump_index]
57                  line=np.hstack((tnow,cv(start)))
58                  wline(file,line)
59                  norm=np.sum(absv(start))
60                  ny=np.random.rand(1)
61                  tnow+=dt
62                  break
63          print(tnow,norm)
64          Dt=dt/np.log(math.sqrt(np.sum(absv(temp[-2])))/math.sqrt(np.sum(
    absv(temp[-1]))))
```

Listing 6.4: time_evo_qj.py

6.5 Time Evolution for Local Noise

```
from Hamilton_full_epsilon import build,H_e,n
from Timeevolution_QJ_sym import timeevo_QJ
import numpy as np
import os
from time import process_time as ptime
from datetime import datetime
from sys import argv
from sym import U_S,transfm,transfv
import pprint

#HAM-parameters
N=24
L=4
U=1
eta=0.3
J=1
J_list=[[J,J*eta],[J,J*eta]]
eps=U*(N/2-1)

#EVO-parameters
t=150
dt=0.05
kappa=[0.6]
startstate=[N/2,0,0,N/2]
#indexlist=[231,421,574,694,785,851,896,924,939,945]


#kappa=[0.05]

#NAME-parameters
path="/remote/lin5a/fischer_d/data/noise_sym/N24/"
#path="C:\\Users\\Rossbach Maler\\Desktop\\auswertung\\test\\"
name=str(argv[1])+"N"+str(N)+"k"+str(kappa)+"J"+str(J)+"eta"+str(eta)

pprint.pprint(locals())


def main():
    basis=build(N,L)
    S=len(basis)
    Ham=H_e(N,U,[0,0,eps,0],J_list,False)
    tm_S,block_i=U_S([[3,1,2,0]],N,L)


    y0=np.zeros([S])
    y0[basis.index(startstate)]+=1
    by0=transfv(y0,tm_S,block_i[1],block_i[2])


    bham=transfm(Ham,tm_S,block_i[1],block_i[2])
    bn=transfm(n(2,N,L),tm_S,block_i[1],block_i[2])

    t1=ptime()
    x=np.arange(0,t,dt)
    timeevo_QJ(bham,by0,t,dt,dt*100,kappa,[bn],path+name+".txt")
    t2=ptime()
    print(t2-t1)

main()
```

Listing 6.5: local_noise.py

References

[1] Georgios Kordas, Dirk Witthaut, and Sandro Wimberger. "Non-equilibrium dynamics in dissipative Bose-Hubbard chains". In: *Annalen der Physik* (2015). ISSN: 1521-3889. DOI: 10.1002/andp.201400189.

[2] Andrea Tomadin, Riccardo Mannella, and Sandro Wimberger. "Many-body Landau-Zener tunneling in the Bose-Hubbard model". In: *Phys. Rev. A* 77 (1 2008), p. 013606. DOI: 10.1103/PhysRevA.77.013606.

[3] Georgios Kordas. "Beyond Mean Field Dynamics in Closed and Open Bosonic Systems". PhD thesis. Universität Heidelberg and National University of Athens, 2013. URL: http://archiv.ub.uni-heidelberg.de/volltextserver/15901/.

[4] Ivana Vidanović, Daniel Cocks, and Walter Hofstetter. "Dissipation through localized loss in bosonic systems with long-range interactions". In: *Phys. Rev. A* 89 (5 2014), p. 053614. DOI: 10.1103/PhysRevA.89.053614.

[5] M. P. Strzys and J. R. Anglin. "Four-mode Bose-Hubbard model with two greatly differing tunneling rates as a model for the Josephson oscillation of heat". In: *Phys. Rev. A* 81 (4 2010), p. 043616. DOI: 10.1103/PhysRevA.81.043616.

[6] Ralf Labouvie, Bodhaditya Santra, Simon Heun, Sandro Wimberger, and Herwig Ott. "Negative differential conductivity in an interacting quantum gas". In: *Phys. Rev. Lett.* in press (2015), preprint: arXiv: 1411.5632.

[7] Heinz-Peter Breuer and Francesco Petruccione. *The theory of open quantum systems*. eng. 1. publ., repr. Oxford: Oxford Univ. Press, 2003, XXI, 625 S. ISBN: 0-19-852063-8 ; 978-0-19-852063-4.

[8] Immanuel Bloch, Jean Dalibard, and Wilhelm Zwerger. "Many-body physics with ultracold gases". In: *Rev. Mod. Phys.* 80 (3 2008), pp. 885–964. DOI: 10.1103/RevModPhys.80.885.

[9] Madan Lal Mehta. *Random matrices*. eng. Rev. and enlarged 2. ed. Boston [u.a.]: Acad. Pr., 1991, XIII, 562 S. ISBN: 0-12-488051-7 ; 978-0-12-488051-1.

[10] Sandro Marcel Wimberger. *Nonlinear dynamics and quantum chaos. an introduction*. eng. Graduate Texts in Physics. Cham ; Heidelberg [u.a.]: Springer, 2014, XIII, 206 S. ISBN: 978-3-319-06342-3 ; 978-3-319-06343-0.

[11] M. V. Berry and M. Tabor. "Level Clustering in the Regular Spectrum". In: *Proc. R. Soc. London A* 356.1686 (1977), pp. 375–394. ISSN: 0080-4630. DOI: 10.1098/rspa.1977.0140.

[12] Y Y Atas, E Bogomolny, O Giraud, P Vivo, and E Vivo. "Joint probability densities of level spacing ratios in random matrices". In: *Journal of Physics A: Mathematical and Theoretical* 46.35 (2013), p. 355204. URL: http://stacks.iop.org/1751-8121/46/i=35/a=355204.

[13] Vadim Oganesyan and David A. Huse. "Localization of interacting fermions at high temperature". In: *Phys. Rev. B* 75 (15 2007), p. 155111. DOI: 10.1103/PhysRevB.75.155111.

[14] Y. Y. Atas, E. Bogomolny, O. Giraud, and G. Roux. "Distribution of the Ratio of Consecutive Level Spacings in Random Matrix Ensembles". In: *Phys. Rev. Lett.* 110 (8 2013), p. 084101. DOI: 10.1103/PhysRevLett.110.084101.

[15] *SciPy Reference V.0.15.1*. 2015. URL: http://docs.scipy.org/doc/scipy-0.15.1/reference/generated/scipy.integrate.odeint.html.

[16] Alan C. Hindmarsh. *Brief Description of ODEPACK*. 2001. URL: http://www.netlib.org/odepack/opkd-sum.

[17] Th. Anker, M. Albiez, R. Gati, S. Hunsmann, B. Eiermann, A. Trombettoni, and M. K. Oberthaler. "Nonlinear Self-Trapping of Matter Waves in Periodic Potentials". In: *Phys. Rev. Lett.* 94 (2 2005), p. 020403. DOI: 10.1103/PhysRevLett.94.020403.

[18] Darius Hoffmann. "The Transition to Chaos in the two-dimensional Bose-Hubbard Model". B.S. Thesis. Universität Heidelberg, 2015.

[19] P. Buonsante and A. Vezzani. "Ground-State Fidelity and Bipartite Entanglement in the Bose-Hubbard Model". In: *Phys. Rev. Lett.* 98 (11 2007), p. 110601. DOI: 10.1103/PhysRevLett.98.110601.

[20] B. Misra and E. C. G. Sudarshan. "The Zeno's paradox in quantum theory". In: *Journal of Mathematical Physics* 18.4 (1977).